European Polymer Journal 65 (2015) 202–208

Contents lists available at ScienceDirect

European Polymer Journal

journal homepage: www.elsevier.com/locate/europolj

Macromolecular Nanotechnology

Generation of large and locally aligned wormlike micelles in block copolymer/epoxy blends

Agustina B. Leonardi, Ileana A. Zucchi, Roberto J.J. Williams *

Institute of Materials Science and Technology (INTEMA), University of Mar del Plata and National Research Council (CONICET), Av. J. B. Justo 4302, 7600 Mar del Plata, Argentina

ARTICLE INFO

Article history:
Received 8 September 2014
Received in revised form 25 October 2014
Accepted 2 November 2014
Available online 7 November 2014

Keywords:
Block copolymer
Hexagonally packed cylinders
Polymerization-induced self-assembly
PS-*b*-PEO/epoxy
Wormlike micelles

ABSTRACT

A dispersion of wormlike micelles, empirically found in some block copolymer (BCP)/epoxy blends, has been reported to produce a significant toughening of epoxy networks. In this study, a rationale procedure to generate and trap large and locally aligned wormlike micelles in an epoxy matrix is reported. A BCP/epoxy/hardener blend was selected that was homogeneous at the polymerization temperature but became nanostructured in the course of polymerization leading to hexagonally packed cylinders (HPC) domains. When a similar BCP with a molar mass about three times larger than the first one and with the same ratio between blocks was used, the nanostructuration into HPC domains was frustrated by diffusional limitations of the large cylindrical micelles generated. A morphology consisting of a dispersion of large and locally aligned wormlike micelles was trapped in the cross-linked epoxy. The selected BCP was polystyrene (PS)-*b*-poly(ethylene oxide) (PEO), with molar masses M = 43 kDa or 136 kDa and a mass fraction of PEO close to 25 wt%. The network precursors were based on diglycidylether of bisphenol A (DGEBA) and 4, 4′-methylenebis(2,6-diethylaniline) (MDEA). Low- and high-molar-mass BCP generated, respectively, HPC domains and wormlike micelles, as supported by TEM images and SAXS spectra.

1. Introduction

Hillmyer et al. [1,2] first reported the use of block copolymers (BCP) to generate nanostructures in epoxy networks. The strategy was to self-assemble a BCP in the precursors of the epoxy network, by selecting one immiscible block and one miscible block from the beginning of reaction up to high conversions. In this way, the initially self-assembled nanostructure could be fixed by the cross-linking reaction. Keeping miscibility of one of the blocks up to high conversions enabled to avoid macrophase separation of the whole BCP. However, at high conversions the initially miscible block can also undergo phase separation leading to the occurrence of ordered-ordered phase transitions at particular concentrations [2]. Zheng and colleagues shown that a similar nanostructuration could result when both blocks are initially miscible in the thermoset precursors but one of the blocks becomes phase separated in the course of polymerization while the other block keeps its miscibility up to high conversions [3,4]. This process was called reaction-induced microphase separation (RIMPS). While the nanostructuration via the self-assembly approach is based on equilibrium thermodynamics of the initial system, for RIMPS the resulting nanostructures depend on the competitive kinetics between polymerization and phase separation. This provides RIMPS with a high versatility to convey the nanostructuration process [4–12].

Regarding the applications of BCP/epoxy blends, focus has been placed on the role of the BCP as a processing

* Corresponding author. Tel.: +54 223 4816600.
E-mail address: williams@fi.mdp.edu.ar (R.J.J. Williams).

http://dx.doi.org/10.1016/j.eurpolymj.2014.11.001
0014-3057/

aid [13,14], as a template for the self-assembly of different type of nanoparticles [15–17], and as toughening agents [18–25]. At low BCP concentrations (<10 wt%), spherical micelles, wormlike micelles or vesicles are generated in the epoxy matrix depending on the ratio of epoxy-philic to epoxy-phobic blocks [18,23,26]. In water solutions the evolution from spherical micelles → wormlike micelles → octopi → jellyfish → vesicles, was observed when increasing the length of the hydrophobic block of the BCP with respect to the hydrophilic one [27]. Wormlike micelles are convenient morphologies for toughening purposes [20–23] (the lack of verification of plane-strain conditions might invalidate some of these results [18]).

Usually, small concentrations of BCP (<5 wt%) are required for a significant toughening of the cured epoxy. In the diluted concentration limit, the composition of the BCP that generates wormlike micelles is difficult to predict [26], but may be empirically found [23]. A paper by Hermel-Davidock et al. [28], illustrates the difficulty in predicting conditions to generate wormlike micelles. They investigated BCP/epoxy formulations where nanostructuration was produced before polymerization. It was shown that the nature of a solvent used to homogenize the initial blend and that was later vaporized, determined the generation of either spherical or wormlike micelles that were trapped in the cured material. For one of the blends, wormlike micelles were generated during polymerization from the evolution of spherical micelles present in the initial material. Several papers reported the presence of wormlike micelles in cured BCP/epoxy blends [20–23,26,29–32]. It is difficult, however, to extract from these studies general rules enabling to obtain wormlike micelles in the final material.

The toughening of high-T_g (glass transition temperature) epoxies with BCP is much more complex. In this case, there is a smaller shear yielding zone ahead of the crack tip determining the need to increase the BCP concentration to allow yielding to take place [25]. However, incorporating large amounts of BCP (>10 wt%) to the epoxy precursors leads to ordered nanostructures such as body-centered cubic (BCC), hexagonally-packed cylinders (HPC), gyroid (G) or lamella (L) [2,33], instead of the desired micelles.

In this article, a rationale procedure to generate and trap wormlike micelles using a 20 wt% BCP in an epoxy matrix is reported, employing the versatility of the RIMPS process. The starting point is a BCP selected in such a way that both blocks are initially miscible in the epoxy/hardener solvent and that generates hexagonally packed cylinder (HPC) domains in the cured material via RIMPS. The way in which HPC domains are generated in the course of polymerization was recently analyzed [12]. Phase separation starts by the formation of spherical micelles that evolve through a BCC structure to micellar columns, then to cylindrical rods that finally form the HPC phase [12]. The driving force of these transformations is the decrease in the reactive solvent affinity for the epoxy-philic block with the increase in conversion, mainly due to the decrease in the entropic contribution to the free energy of mixing [34]. The aim of this study was placed on trapping the morphology at the stage of cylindrical rods (wormlike micelles), avoiding their packing into HPC domains. This should be accomplished by increasing the molar mass of the BCP keeping the same ratio between blocks. Diffusional restrictions for the packing of large cylindrical micelles should avoid the generation of the HPC domains and arrest the nanostructuration at the level of cylindrical micelles.

The selected BCP to investigate this hypothesis was polystyrene (PS)-*b*-poly(ethylene oxide) (PEO), with two different molar masses M = 43 kDa or 136 kDa and a mass fraction of PEO close to 25 wt%. The network precursors were based on diglycidylether of bisphenol A (DGEBA) and 4,4′-methylenebis(2,6-diethylaniline) (MDEA). In this system, PEO is the epoxy-philic block and PS is the epoxy-phobic block that is initially miscible at the polymerization temperature (135 °C) but phase separates during polymerization [12]. The solubility of PEO in the reactive solvent decreases with conversion leading to an evolution of the nanostructures. It is also known that the solubility of PEO arises from H-bonds formed among ether groups of PEO and OH groups generated in the epoxy-amine reaction [4,35,36]. A temperature increase should decrease its solubility by a decrease in the fraction of H-bonded ether groups (LCST, lower-critical-solution temperature behavior). Cured samples were subjected to a prolonged thermal treatment at 190 °C to investigate a possible effect of PEO insolubility on the nanostructures generated at 135 °C.

2. Experimental section

2.1. Materials

The epoxy monomer was based on diglycidylether of bisphenol A (DGEBA), with an epoxy equivalent of 179 g/mol, determined by chemical titration. The hardener was 4,4′-methylenebis(2,6-diethylaniline) (MDEA, Aldrich), used in an almost stoichiometric proportion (stoichiometric epoxy/amine ratio equal to 0.974 in equivalents of both monomers). Two commercial polystyrene (PS)-*b*-poly(ethylene oxide) (PEO) BCP (Polymer Source) were selected. The low-molar-mass BCP, L-BCP, had a number average molar mass, M_n = 43000 Da (PS = 32,000 Da and PEO = 11,000 Da), and a polydispersity index, PI = 1.06. The high-molar-mass BCP, H-BCP, had M_n = 136,000 Da (PS = 102,000 Da and PEO = 34,000 Da), and PI = 1.18. Therefore, H-BCP had about three times the molar mass of L-BCP but the same fraction of PEO blocks (about 25 wt%). A PEO homopolymer (M_n = 13,000 Da and PI = 1.10, Polymer Source) was employed to analyze the effect of a prolonged thermal treatment at 190 °C on its solubility in the epoxy network.

2.2. Synthesis and cure of blends

First, DGEBA was blended with either PEO, L-BCP or H-BCP, in proportions giving 20 wt% of modifier in the final cured material. The dissolution was performed in a silicon mold adding a small amount of toluene to facilitate the process. Toluene was then removed at 80 °C during several hours until a constant weight was obtained. Then, MDEA was added with continuous stirring. The polymerization was carried out at 135 °C during 4 h. The nanostructures

generated were analyzed at this stage and after a thermal treatment at 190 °C for another 4 h under nitrogen.

2.3. Characterization techniques

Differential scanning calorimetry (DSC) thermograms were obtained at a heating rate of 20 °C/min under nitrogen flow, using a DSC Perkin–Elmer Pyris 1. Glass transition temperatures (T_g) were taken at the mid-value of the change in the specific heat and melting temperatures were defined at the minimum of the melting peak.

Middle-infrared spectroscopy was used to investigate the evolution of H-bonds in PEO/epoxy-amine blends during polymerization at 135 °C as well as the influence of temperature on the fraction of H-bonds in cured materials. A Nicolet 6700 FTIR device, equipped with a heated transmission cell (HT-32, Spectra Tech) with NaCl windows (32 mm diameter), and a programmable temperature controller (Omega, Spectra Tech, DTZG1 8C), was employed.

Transmission Electron Microscopy (TEM) images were recorded at room temperature using a JEOL 100CX device. Thin sections were obtained employing an LKB ultramicrotome. PS blocks appeared black in the images and therefore no staining procedure was necessary.

Small-Angle X-ray Scattering (SAXS) spectra were obtained at the beamline SAXS 1 of the National Laboratory of Synchrotron Light (LNLS, Campinas, Brazil). The scattering intensity (in arbitrary units) was recorded as a function of the scattering vector $q = (4\pi/\lambda)\sin\theta$, where λ is the radiation wavelength (1.55 A) and 2θ the scattering angle.

3. Results and discussion

3.1. Thermal characterization of the BCP

Both BCP were characterized by DSC to analyze the variation of the melting peak of PEO with its molar mass, a necessary information for the discussion of results shown in next section. Fig. 1 shows DSC thermograms for the BCP of low (L-BCP) and high (H-BCP) molar masses.

The melting point of PEO in L-BCP (M_n PEO = 11,000 Da) is 51.5 °C while in H-BCP (M_n PEO = 34,000 Da) it is 65 °C. The glass transition temperature of the PS blocks is also present in both thermograms (inset in Fig. 1).

3.2. Influence of temperature on the solubility of PEO in the cured epoxy network

While the amount of PEO in blends containing 20 wt% BCP was only 5.9 wt% with respect to the epoxy/amine network, a blend containing 20 wt% PEO was used to investigate the effect of temperature on its miscibility with the cured epoxy network. The evolution of FTIR spectra taken *in situ* during polymerization at 135 °C, was followed in the region of the OH stretching vibration (Fig. 2).

After 40 min reaction, the spectrum exhibited two well-defined peaks at 3390 cm^{-1} (assigned to H-bonded OH and ether groups) and at 3480 cm^{-1} (assigned to H-bonded OH groups) [4], and a shoulder at about 3580 cm^{-1} (assigned to isolated OH groups). The generation of OH groups by the epoxy-amine reaction produced a continuous increase in the intensity of the band assigned to H-bonded OH groups as well as a shift to lower wavenumbers. The band assigned to the interaction of ether groups of PEO with hydroxyls remained as a clear shoulder after 200 min reaction.

Samples were cured 4 h at 135 °C followed by 4 h at 190 °C. FTIR spectra of the cured blend recorded at various temperatures are shown in Fig. 3. In the spectrum taken at 190 °C, a significant decrease of the shoulder at 3390 cm^{-1} was observed together with an increase in the intensity of a peak assigned to isolated OH groups. This implies that at 190 °C there was a significant decrease of the miscibility of PEO with the epoxy/amine network. Decreasing temperature to room temperature produced a continuous increase in the solubility of PEO as revealed by the evolution of FTIR spectra. This behavior was totally reversible implying that the polymer network behaved as a good solvent of PEO at room temperature and as a poor solvent at 190 °C.

The question whether the epoxy network became a non-solvent (rather than a poor solvent) at 190 °C was difficult to answer because samples remained transparent without any visual evidence of phase segregation at the scale of optical microscopy. However, a calorimetric study provided an answer to this question. Fig. 4 shows DSC thermograms of the sample obtained after the 4 h heating at 190 °C, in first and second heating scans. In the first scan, a small melting peak at 57 °C is present, followed by a broad glass transition temperature placed at about 80 °C. The small melting peak lies in the expected temperature range for PEO with M_n = 13,000 Da (as discussed in the previous section melting peaks for PEO in the BCP were 51.5 °C for M_n = 11,000 Da and 65 °C for M_n = 34,000 Da). However, the fraction of crystallized PEO was significantly small. Taking a value of 205 J/g for the heat of fusion of PEO crystals [37], led to a 2.9 % crystalline fraction of the added PEO. Crystals were dissolved in the first heating scan and crystallization did not occur when cooling before performing the second heating scan. These results may be interpreted as follows. At 190 °C the epoxy/amine network became a non-solvent for PEO and partial phase separation took place after the prolonged heating at this temperature. When cooling to room temperature, phase separated PEO was not completely re-dissolved and it crystallized. In the first DSC heating scan PEO crystals were melted and re-dissolved in the epoxy network. As the sample was immediately cooled after the first scan, phase separation of PEO did not take place and no crystallinity was observed in the second scan. Most of the PEO remained soluble in the epoxy network significantly decreasing its glass transition temperature from 150 °C (see next section), to about 80 °C.

The decrease in the solvent quality for the PEO brushes present in the nanostructured BCP might produce morphological changes including an order-order phase transition, as discussed by Lipic et al. [2]. Therefore, a 4 h heating at 190 °C was performed in the cured BCP/epoxy blends to analyze this possibility.

3.3. Calorimetric characterization of BCP/epoxy networks after cure

Fig. 5 shows DSC thermograms for the neat matrix after the cure (4 h at 135 °C plus 4 h at 190 °C), and for the

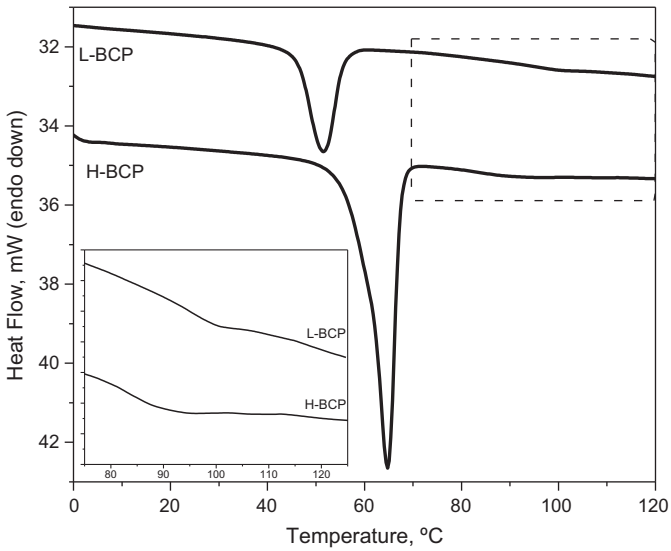

Fig. 1. DSC thermograms of L-BCP and H-BCP.

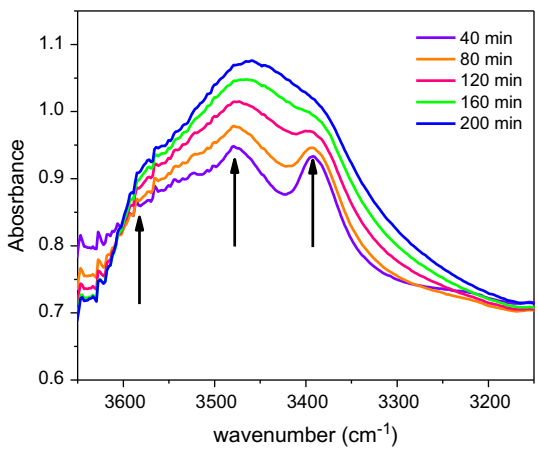

Fig. 2. Evolution of FTIR spectra in the region of the OH stretching vibration for a blend containing 20 wt% PEO, taken *in situ* during polymerization at 135 °C.

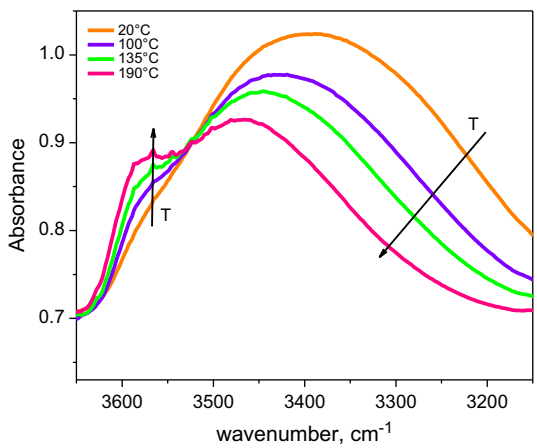

Fig. 3. Evolution of FTIR spectra in the region of the OH stretching vibration for a cured blend containing 20 wt% PEO, when increasing temperature from 20 °C to 190 °C. A reversible transformation was observed in a cooling step from 190 °C to 20 °C.

blends containing 20 wt% L-BCP and H-BCP after 4 h at 135 °C and after another 4 h at 190 °C.

Regarding the cured epoxy network, as its glass transition was close to 150 °C, the polymerization was arrested by vitrification at 135 °C. Therefore, it was necessary to post-cure at 190 °C to rich full conversion. Values higher than 150 °C have been reported for the maximum glass transition temperature of stoichiometric DGEBA-MDEA networks (e.g., T_g = 180 °C, defined in the same way [38]). These higher values of glass transition temperatures were obtained for practically pure diglycidylether of bisphenol A used in a strict stoichiometric proportion. This was not the case for our epoxy monomer, added to the fact that it was used in a small defect with respect to stoichiometry as indicated in the Experimental Section. Besides, the use of a DGEBA containing a significant fraction of OH groups led to an acceleration of the reaction compared to the slow kinetics recorded at 135 °C when using practically pure diglycidylether of bisphenol A [12]. Therefore, it was possible to cure blends containing 20 wt% BCP to high conversions after 4 h at 135 °C. No significant changes in the glass transition temperature of BCP/epoxy blends were observed before and after the thermal treatment at 190 °C (Fig. 5). The T_g values of the plasticized epoxy networks were lower than the polymerization temperature so that vitrification did not play any effect on the reaction at 135 °C.

3.4. Generation of HPC domains in BCP/epoxy networks

The selected low-molar-mass PS-*b*-PEO (L-BCP) was nanostructured as hexagonally packed cylinder (HPC) domains after the first stage of polymerization at 135 °C.

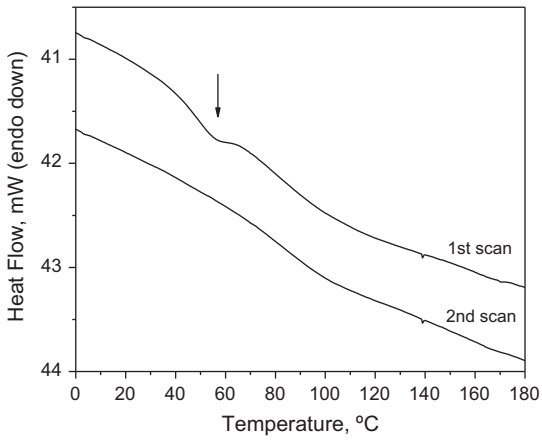

Fig. 4. First and second DSC heating scans for a blend containing 20 wt% PEO after the thermal treatment at 190 °C.

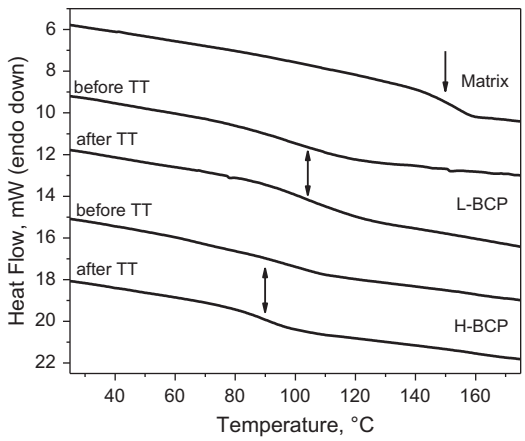

Fig. 5. DSC thermograms for the neat matrix after the cure (4 h at 135 °C plus 4 h at 190 °C), and for the blends containing 20 wt% L-BCP and H-BCP, after 4 h at 135 °C and after another 4 h at 190 °C (TT = thermal treatment).

The resulting morphology did not change after the thermal treatment at 190 °C, meaning that the partial shrinkage of PEO brushes at high temperatures had no significant effect. Fig. 6 shows a TEM image of the blend after the thermal treatment. PS cylinders (in black) are hexagonally packed in a PEO/epoxy continuous medium (in grey). Disordered regions alternate with HPC domains. This arises from the need to balance the mass fraction of BCP in both regions with the one added to the initial formulation.

Fig. 7 shows SAXS spectra obtained after the cure at 135 °C and after the thermal treatment at 190 °C. There was no change in SAXS spectra after the thermal treatment evidencing again that the partial shrinkage of PEO coils did not affect the HPC phase generated at 135 °C.

Two sets of characteristic peaks may be distinguished in the SAXS spectra of Fig. 7. The first most intense peak ($q_{100} = 0.154\ nm^{-1}$) and the shoulder at $q/q_{100} = \sqrt{3}$, are characteristic peaks of the HPC structure. The third peak overlaps peaks of the HPC structure with the first peak of

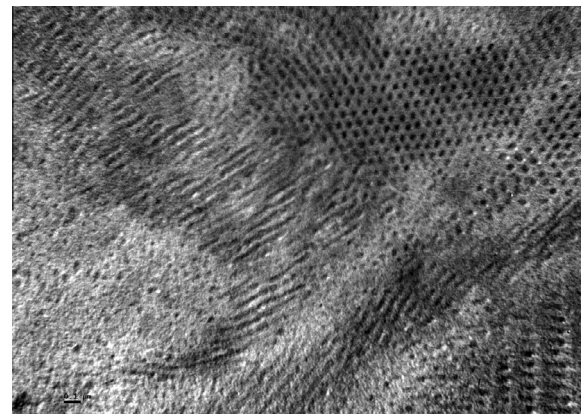

Fig. 6. TEM image showing HPC domains generated in the L-BCP/epoxy blend. The black bar at the left indicates 100 nm.

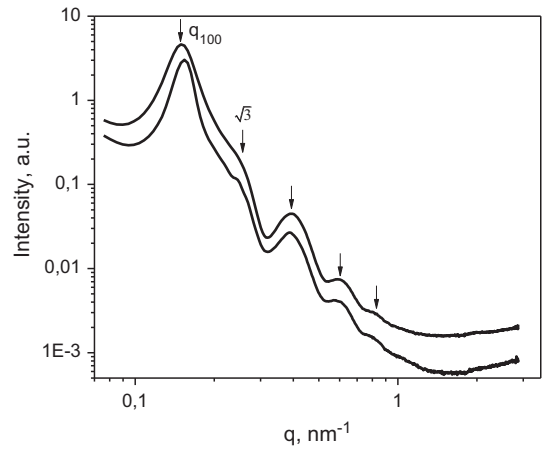

Fig. 7. SAXS spectra of the L-BCP/epoxy blend obtained after the cure at 135 °C (upper curve) and after the thermal treatment at 190 °C (lower curve).

the form factor of cylinders (expected in the sequence $qR = 4.98, 8.364, 11.46\ldots$, where R is the radius of cylinders) [39]. The two small peaks marked with arrows at q values of 0.60 $nm^{-1}$and 0.82 nm^{-1}, lie in the expected sequence for the second and third peaks of the form factor of cylinders. The diameter of cylinders may be calculated as $D = 2 \times 8.364/0.60 = 28$ nm which is close to the one estimated from the TEM image. The volume fraction of cylinders in the HPC structure (f_{HPC}) may be calculated from: $f_{HPC} = (\pi\sqrt{3}/2)(R/d_{100})^2$, where $d_{100} = 2\pi/q_{100}$ [39]. This gives $f_{HPC} = 0.32$, a value that doubles the PS volume fraction added to the initial formulation. The presence of disordered regions containing a low BCP concentration balances the overall BCP concentration in the blend with respect to its initial concentration.

3.5. Generation of wormlike micelles in BCP/epoxy networks

The starting hypothesis was that increasing the molar mass of the BCP and keeping the same ratio between

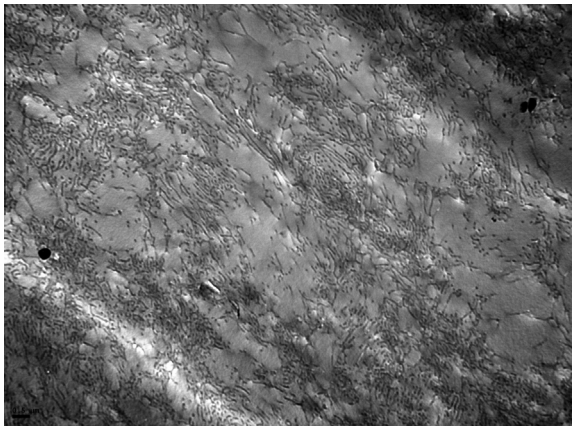

Fig. 8. Wormlike micelles generated in the 20 wt% H-BCP/epoxy blend after the cure at 135 °C. The black bar at the left indicates 500 nm.

blocks could generate large cylindrical rods that would not be able to self-assemble into HPC domains due to diffusional limitations. This hypothesis was checked replacing L-BCP by H-BCP that had a molar mass three times larger and kept the same ratio of blocks.

Figs. 8 and 9 show, respectively, TEM images of nanostructures generated after the polymerization stage at 135 °C and after the thermal treatment at 190 °C.

Both TEM images look similar indicating again that the thermal treatment did not produce any significant modification of the nanostructure generated during the cure at 135 °C. A large concentration of wormlike micelles was observed in the whole area of samples. The length of the observed micelles depends on the angle they formed with respect to the direction of the cut. Those located in the plane of the cut exhibit lengths of several microns. The frustrated formation of HPC domains is evidenced by their clustering and local alignment as well as by the fact that there is a partial depletion of micelles in other areas.

In a previous paper [12] we followed the evolution of the nanostructuration of a polystyrene (PS)-*b*-poly(methyl methacrylate) (PMMA) BCP in a similar matrix. We showed that columns of spherical micelles generated cylinders that packed into HPC domains. For very long cylindrical micelles as those produced by H-BCP, the last step of this ordering process did not take place due to the unfavorable competition between diffusion and polymerization kinetics (Fig. 10). Therefore, nanostructuration was arrested at the step of clustering and local alignment of the long cylinders.

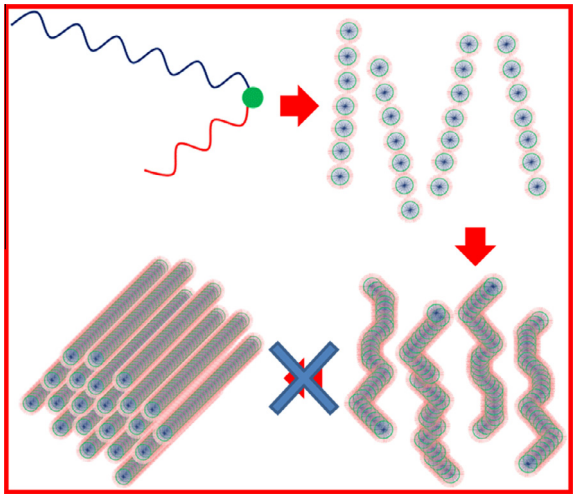

Fig. 10. Scheme of the generation of locally aligned cylindrical micelles.

In spite of the relatively large size of the wormlike micelles, nanocomposites were completely transparent. Possibly, the close value of refractive indices of PS and the cured epoxy helped to keep transparency [40,41].

SAXS spectra taken before and after the thermal treatment were similar (Fig. 11).

The first and second peaks marked by arrows in the SAXS spectra are located at q values close to 0.15 $nm^{-1}$and 0.25 nm^{-1}. These values are in the expected sequence of the first and second peaks of the form factor of cylinders. The diameter of cylinders calculated from the first peak

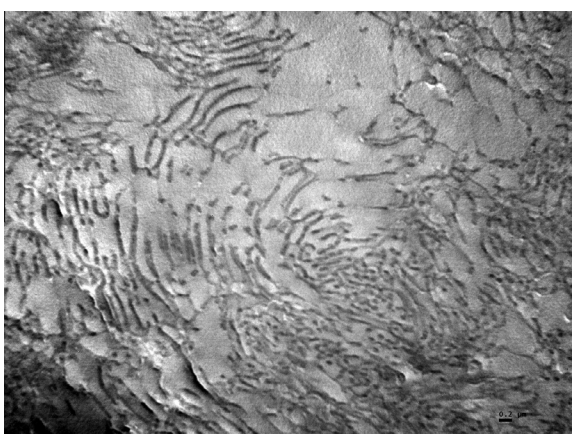

Fig. 9. Wormlike micelles generated in the 20 wt% H-BCP/epoxy blend after the thermal treatment at 190 °C. The black bar at the right indicates 200 nm.

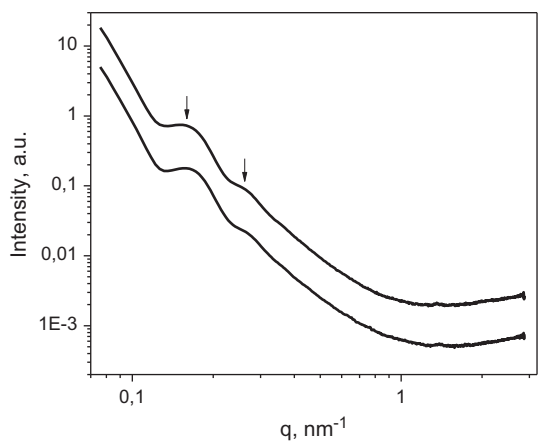

Fig. 11. SAXS spectra of the H-BCP/epoxy blend obtained after the cure at 135 °C (upper curve) and after the thermal treatment at 190 °C (lower curve).

is D = 66 nm, in agreement with the value estimated from TEM images. Then, increasing the molar mass of PS blocks by a factor of 3.2 increased the diameter of cylinders by a factor 2.4. The difference was that in the first case the cylinders were self-assembled into HPC domains whereas in the second case they were present as locally aligned wormlike micelles.

4. Conclusions

A procedure to generate a large concentration of locally aligned wormlike micelles in BCP/epoxy blends, was presented. It is based on selecting a BCP with a ratio of blocks that generates HPC domains but with a high molar mass that frustrates the self-assembly of the large cylindrical micelles generated during polymerization due to diffusional restrictions. In this way, a large concentration of locally aligned wormlike micelles is generated in the cured blend. The procedure was illustrated using a large molar mass PS-*b*-PEO initially dissolved in a DGEBA-MDEA formulation.

Acknowledgments

We acknowledge the financial support of the University of Mar del Plata (Argentina), the National Research Council (CONICET, Argentina) and the National Agency for the Promotion of Science and Technology (ANPCyT, Argentina). The grant SAXS1-13459 from the Brazilian Synchrotron Light Laboratory (LNLS, Campinas, Brazil) is gratefully acknowledged.

References

[1] Hillmyer MA, Lipic PM, Hajduk DA, Almdal K, Bates FS. J Am Chem Soc 1997;119:2749–50.
[2] Lipic PM, Bates FS, Hillmyer MA. J Am Chem Soc 1998;120:8963–70.
[3] Meng F, Zheng S, Zhang W, Li H, Liang Q. Macromolecules 2006;39:711–9.
[4] Meng F, Zheng S, Li H, Liang Q, Liu T. Macromolecules 2006;39:5072–80.
[5] Serrano E, Martin MD, Tercjak A, Pomposo JA, Mercerreyes D, Mondragon I. Macromol Rapid Commun 2005;26:982–5.
[6] Serrano E, Tercjak A, Kortaberria G, Pomposo JA, Mercerreyes D, Zafeiropoulos NE. Marcromolecules 2006;39:2254–61.
[7] Serrano E, Tercjak A, Ocando C, Larrañaga M, Parellada MD, Corona-Galván S, et al. Macromol Chem Phys 2007;208:2281–92.
[8] Fang W, Zheng S. Polymer 2008;49:3157–67.
[9] Serrano E, Kortaberria G, Arruti P, Tercjak J, Mondragon I. Eur Polym J 2009;45:1046–57.
[10] Hu D, Zheng S. Eur Polym J 2009;45:3326–38.
[11] Yu R, Zheng S. Macromolecules 2011;44:8546–57.
[12] Romeo HE, Zucchi IA, Rico M, Hoppe CE, Williams RJJ. Macromolecules 2013;46:4854–61.
[13] Girard-Reydet E, Pascault JP, Bonnet A, Court F, Leibler L. Macromol Symp 2003;198:309–22.
[14] Fine T, Inoubli R, Gérard P, Pascault JP. In: Pascault JP, Williams RJJ, editors. Epoxy polymers: new materials and innovations. Weinheim: Wiley-VCH; 2010. p. 289–302.
[15] Nandan B, Kuila BK, Stamm M. Eur Polym J 2011;47:584–99.
[16] Gutierrez J, Mondragon I, Tercjak A. Polymer 2011;52:5699–707.
[17] Tercjak A, Gutierrez J, Martin MD, Mondragon I. Eur Polym J 2012;48:16–25.
[18] Ruiz-Pérez L, Royston GJ, Fairclough JPA, Ryan AJ. Polymer 2008;49:4475–88.
[19] Zheng S. In: Pascault JP, Williams RJJ, editors. Epoxy polymers: new materials and innovations. Weinheim: Wiley-VCH; 2010. p. 81–108.
[20] Dean JM, Verghese NE, Pham HQ, Bates FS. Macromolecules 2003;36:9267–70.
[21] Wu J, Thio YS, Bates FS. J Polym Sci, Part B: Polym Phys 2005;43:1950–65.
[22] Thio YS, Wu J, Bates FS. Macromolecules 2006;39:7187–9.
[23] Liu J, Thompson ZJ, Sue HJ, Bates FS, Hillmyer MA, Dettloff M, et al. Macromolecules 2010;43:7238–43.
[24] Declet-Perez C, Redline EM, Francis LF, Bates FS. ACS Macro Lett 2012;1:338–42.
[25] Redline EM, Declet-Perez C, Bates FS, Francis LF. Polymer 2014;55:4172–81.
[26] Guo Q, Dean JM, Grubbs RB, Bates FS. J Polym Sci, Part B: Polym Phys 2003;41:1994–2003.
[27] Blanazs A, Madsen J, Battaglia G, Ryan AJ, Armes SP. J Am Chem Soc 2011;133:16581–7.
[28] Hermel-Davidock TJ, Tang HS, Murray DJ, Hahn SF. J Polym Sci, Part B: Polym Phys 2007;45:3338–48.
[29] Guo Q, Thomann R, Gronski W, Thurn-Albrecht T. Macromolecules 2002;35:3133–44.
[30] Gerard P, Passade Boupat N, Fine T, Gervat L, Pascault JP. Macromol Symp 2007;256:55–64.
[31] Ocando C, Serrano E, Tercjak A, Peña C, Kortaberria G, Calberg C, et al. Macromolecules 2007;40:4068–74.
[32] Cano L, Builes DH, Tercjak A. Polymer 2014;55:738–45.
[33] Dean JM, Lipic PM, Grubbs RB, Cook RF, Bates FS. J Polym Sci, Part B: Polym Phys 2001;39:2996–3010.
[34] Williams RJJ, Rozenberg BA, Pascault JP. Adv Polym Sci 1997;128:95–156.
[35] Zheng S, Zhang N, Luo X, Ma D. Polymer 1995;36:3609–13.
[36] Guo Q, Harrats C, Groeninckx G, Koch MHJ. Polymer 2001;42:4127–40.
[37] Zheng H, Zheng S, Guo Q. J Polym Sci, Part A: Polym Chem 1997;35:3161–8.
[38] Di Luca C, Soulé ER, Zucchi IA, Hoppe CE, Fasce LA, Williams RJJ. Macromolecules 2010;43:9014–21.
[39] Hashimoto T, Kawamura T, Harada M, Tanaka H. Macromolecules 1994;27:3063–72.
[40] Hoppe CE, Galante MJ, Oyanguren PA, Williams RJJ, Girard-Reydet E, Pascault JP. Polym Eng Sci 2002;42:2361–8.
[41] Rico M, López J, Montero B, Bellas R. Eur Polym J 2012;48:1660–73.